International Journal of Automotive Technology, Vol. 14, No. 2, pp. 221−231 (2013)
DOI 10.1007/s12239−013−0025−z

pISSN 1229−9138/ eISSN 1976−3832

DYNAMIC SENSOR ZEROING ALGORITHM OF 6D IMU MOUNTED ON GROUND VEHICLES

J. OH and S. B. CHOI*

Mechanical Engineering Department, KAIST, Korea Advanced Institute of Science and Technology, Daejeon 305-701, Korea

(Received 13 March 2012; Revised 10 October 2012; Accepted 12 November 2012)

ABSTRACT−The main focus of this paper is to compensate the steady state offset error of the 6D IMU which provides the measurements that include the vehicle linear accelerations and angular rates of all three axes. Additionally, the sensor compensation algorithm exploits the wheel speed data and the steering angle information, since they are already available in most of the modern mass production vehicles. These inputs are combined with the inverse vehicle kinematics to estimate the steady state offset error of each sensor inputs as it is done in a disturbance observer, and the raw sensor measurements are compensated by the estimated offset errors. The stability of the error dynamics regarding the integrated signal processing system is verified, and finally, the performance of the system is tested via experiments based on a real production SUV.

KEY WORDS : Accelerometer, Angular velocities, Calibration, Observers, Stability analysis, Vehicle dynamics

NOMENCLATURE

m : vehicle mass
g : gravitational constant
l_f : distance between C.G. and front axle
l_r : distance between C.G. and rear axle
I_z : moment of inertia about z-axis
C_f : front tire cornering stiffness
C_r : rear tire cornering stiffness
β : side slip angle at C.G
v_x : longitudinal velocity at C.G.
v_y : lateral velocity at C.G.
v_z : vertical velocity at C.G.
a_x : longitudinal acceleration measured at C.G.
a_y : lateral acceleration measured at C.G.
a_z : vertical acceleration measured at C.G
ϕ : roll angle
θ : pitch angle
ψ : yaw angle
p : roll rate measured at C.G.
q : pitch rate measured at C.G.
r : yaw rate measured at C.G.
g_f : front tire steering angle

1. INTRODUCTION

Thanks to the advancement of computerized technology, the prevalence of ground vehicles is nowadays followed by the aid of electronic safety systems, not only as an option but rather as an indispensable part of the car. Here, in order to secure the robust operation of such safety control systems or localization systems (Kim *et al*., 2004; Li *et al*., 2005; Cho and Choi, 2005; Cho *et al*., 2006; Noureldin *et al*., 2009), the sensors mounted on vehicle must provide reliable measurements that interact with the safety control algorithms in a desired manner. In many cases, one or more sets of inertial measurement units (IMU) are used for this purpose, and unfortunately, it must be admitted that highly reliable sensors are only available at a high cost.

If the ideal sensors can be chosen to be mounted on vehicles, free from the cost issue, then the needs for the signal processing algorithm, or even the vehicle state estimation algorithm can all be omitted. However, unless the scope of vehicle production is solely on displaying the state-of-art technology, such choice is not an option. Hence, breaking the tradeoff between the high-performance sensor systems and cost reduction of the mass production cars remains in the role of the signal processing algorithm.

This paper thus focuses on the method to process the sensor signals to minimize the range of error. By doing so, the steady state offset error of the sensor measurements can be significantly reduced. It is true that the sensors of an affordable price comprise various types of limitation other than the offset error, such as the measurement nonlinearity and cross-axis error. However, correction of the offset error is one of the most critical factors to avoid the signal drift issue, especially when integration is involved in the sensor kinematics for the desired state estimation. The simple use of a forgetting factor in integration or high pass filter may help, but only at the cost of severe phase lag and deteriora-

**Corresponding author.* e-mail: sbchoi@kaist.ac.kr

tion of estimation accuracy.

Appealing to such background, one of the most inexpensive sensors is chosen to prove the worthiness of the sensor signal processing methodology and the vehicle observer design that may follow it. The main contribution that distinguishes this paper from others is the sensor offset error correction which is independent of attitude initialization or GPS signals. Also, another unique contribution is the ability to perform reliable sensor offset correction under the influence of severe vehicle motions and attitudes. Such performance is obtained through the use of the lateral velocity estimation from the vehicle model-based observer which utilizes the compensated lateral acceleration measurement, and the stability of this coupled dynamics is analyzed to guarantee accurate sensor offset error identification without steady state error. This unique attempt has not been used in the previous works of the similar interest (Tanaka and Kazumi, 1996; Rogers, 1997; Begin and Cheok, 1998; Shin, 2001; Shin and El-Sheimy, 2004; Abdel-Hamid *et al*., 2006) that require additional sensor information or GPS corrections, or involve shortcomings regarding the disturbance of severe vehicle motion and attitudes. Similar work has been proposed in (Oh *et al*., 2013) on which this work is based, but it lacked in the evidences of experimental validation using an actual vehicle.

The basic organization of this paper is as follows. Section II gives the specification data of an inexpensive 6D IMU that is used for the experiment, and states the need for the sensor compensational algorithm by defining the problem. Section III briefly deals with the principle behind the primary longitudinal velocity approximation based on the wheel angular velocities, and the bicycle model-based observer design that estimates the lateral velocity. Section IV focuses on the dynamic sensor zeroing (DSZ) procedures and the conditions related with them. In section V, the coupled dynamics involved in the dynamic sensor zeroing process is proven to be robust through the stability analysis. Finally, section VI displays the results of the real car-based experiments performed under various different scenarios to verify the effectiveness of sensor offset compensation, after giving a thorough description of the test environments.

2. IMU SPECIFICATION

Given in Table 1 and 2 are the specification data of the sensors used in this research.

Among the specified limitations of the sensors, the offset errors – calibrated null, in case of the gyroscope, and initial 0 g output deviation, in case of the accelerometer – can serve the major difficulty in integrating the sensor signals as mentioned. For instance, purely integrating the accelerometer and gyroscope measurements numerically with the largest offset within the error range for 5 seconds results in the errors of approximately 1.2 m/s in velocity and 15 degrees in angle. Considering that the vehicle lateral velocity and roll angle normally stay within ±1 m/s and ±3 degrees during a mildly driving condition, these error values far exceed what is allowable.

Table 1. Gyroscope specification data.

Analog Devices, Inc. Gyroscope ADW22307					
Parameter	**Conditions**	**Min.**	**Typ.**	**Max.**	**Unit**
Measurement range	F.S. over Specifications range	±250			°/s
Sensitivity		6.2	7	7.8	mV/°/s
Cross axis sensitivity			±1	±3	%
Nonlinearity	% of F.S.		0.1		%
Calibrated null				±3	°/s
Linear acceleration effect	Any axis		0.1		°/s/*g*
Rate noise density	T≤25°C		0.03		°/s/√Hz
Rate noise density	T≤85°C			0.06	°/s/√Hz

Table 2. Accelerometer specification data.

Analog Devices, Inc. Accelerometer ADXL103					
Parameter	**Conditions**	**Min.**	**Typ.**	**Max.**	**Unit**
Measurement range		±1.7			*g*
Sensitivity		960	1000	1040	mV/*g*
Cross axis sensitivity			±1.5	±3	%
Nonlinearity	% of F.S.		±0.2	±1.25	%
Alignment error			±1		Degrees
Initial 0 g output deviation from ideal			±25		m*g*
Output noise	<4 kHz		1	3	mV rms
Noise density			110		μg/√Hz rms

3. OBSERVER DESIGN

3.1. Longitudinal Velocity Estimation

Recent production vehicles provide the individual wheel speeds through the vehicle CAN. Given these four wheel speeds, the velocities at the four corners of the vehicle are available, assuming that there is no longitudinal or lateral wheel slip involved. However, the absence of wheel slip is only true under an extremely limited condition, and these wheel velocities cannot be served directly as an accurate source of information for the longitudinal velocity without a process of refinement.

Reliability of the wheel speed varies inversely with the amount of slip, so it is sensible to take the undriven wheel speed as the value close to the actual longitudinal velocity when the vehicle is accelerating. For the similar reason, the maximum wheel speed is taken when brake is applied. These are patched together, and the result is filtered again with the rate limiter. The rate limiter limits the patched result with respect to the physical limits at which the vehicle can accelerate or decelerate, as well as the longitudinal acceleration value a_x obtained from the 6D IMU. The result, v_{car}, is merely a reference value that is used in the following subcomponents of the observer. It must be clarified that v_{car} is not the final estimated longitudinal velocity.

3.2. Bicycle Model-based Observer

Modeling of the vehicle lateral dynamics is expressed as the following according to the bicycle model.

$$\dot{x} = Ax + Bu \tag{1}$$

$$A = \begin{bmatrix} a_{11} & a_{12} \\ a_{21} & a_{22} \end{bmatrix} = \begin{bmatrix} -\dfrac{2(C_f + C_r)}{mv_x} & \dfrac{-2(C_f l_f - C_r l_r)}{mv_x^2} - 1 \\ \dfrac{-2(C_f l_f - C_r l_r)}{I_z} & -\dfrac{2(C_f l_f^2 + C_r l_r^2)}{I_z v_x} \end{bmatrix},$$

$$\text{and } B = \begin{bmatrix} b_1 \\ b_2 \end{bmatrix} = \begin{bmatrix} \dfrac{2C_f}{mv_x} \\ \dfrac{2C_f l_f}{I_z} \end{bmatrix}$$

Concerning the implementation of the bicycle model shown in (1), the cornering stiffness C_f and C_r henceforth denote those obtained by the cornering stiffness adaptation scheme dealt in (You *et al*., 2009).

The lateral acceleration is expressed as the following.

$$a_y = \dot{v}_y + rv_x \tag{2}$$

Through substituting the right hand side of (2) with the terms used in (1), the lateral acceleration can finally be expressed as shown in (3) (Son, 2008).

$$a_y = a_{11} v_x \beta + (a_{12} + 1) v_x r + b_1 v_x \delta_f \tag{3}$$

To clarify the matters, it must be noted that the lateral acceleration a_y is the vehicle acceleration value with respect to the lateral road surface, instead of the vehicle coordinate. In order to achieve this, sensor reading for the lateral acceleration is processed so that the gravity effect of the suspension roll angle, and pitch angle are eliminated. However, the effect of the road bank or inclination angle must not be eliminated. While the influence of gravity reading due to the suspension angle leads to the false notion that the lateral acceleration exist, the influence of gravity reading due to the road angle must be maintained because it actually affects the vehicle lateral dynamics.

Therefore, a proper compensation of the lateral acceleration sensor measurement is possible only when the separate pieces of information on the pure suspension angles and the road angles are available. In order to obtain both suspension and road angle information, the suspension angles are obtained first by the open loop estimation based on the spring damper system model, and they are subtracted from the total roll and pitch angles estimated in (Oh and Choi, 2011) to estimate the static road angles. Compensation of the lateral acceleration sensor reading is done as follows:

$$a_y = a_{y,sensor} + (-g\sin\phi\cos\theta + g\sin\phi'\cos\theta') \tag{4}$$

$$\text{where } \begin{cases} \phi = \phi' + \phi_{sus} \\ \theta = \theta' + \theta_{sus} \end{cases}$$

Here, ϕ, ϕ', ϕ_{sus}, θ, θ', and θ_{sus} are total roll, static road bank, pure suspension roll, total pitch, static road inclination, and pure suspension pitch angle, respectively.

Besides, the possible influence of the vehicle vertical motion is not considered in the bicycle model observer, since its contribution is assumed to be negligible.

Making use of (2) and choosing the yaw rate and the lateral acceleration as the system outputs, the following estimated output equations can be set up.

$$\hat{y} = C\hat{x} + Du \tag{5}$$

$$\text{where } \hat{y} = \begin{bmatrix} \hat{r} \\ \hat{a}_y \end{bmatrix}, x = \begin{bmatrix} \hat{\beta}_{bic} \\ \hat{r} \end{bmatrix}, \; C = \begin{bmatrix} 0 & 1 \\ a_{11} v_x & (a_{12} + 1) v_x \end{bmatrix}, \text{ and } D = \begin{bmatrix} 0 \\ b_1 v_x \end{bmatrix}$$

With these, and substituting the longitudinal velocity with that estimated based on the wheel dynamics, the following observer is designed.

$$\dot{\hat{x}} = A\hat{x} + Bu + K(y - \hat{y}) \tag{6}$$

By letting

$$K = \begin{bmatrix} K_1 & K_2 \\ K_3 & K_4 \end{bmatrix},$$

Expanding (6) gives the following:

$$\begin{bmatrix} \dot{\hat{\beta}}_{bic} \\ \dot{\hat{r}} \end{bmatrix} = \begin{bmatrix} a_{11} - K_2 a_{11} v_{car} & a_{12} - K_1 - K_2 (a_{12} + 1) v_{car} \\ a_{21} - K_4 a_{11} v_{car} & a_{22} - K_3 - K_4 (a_{12} + 1) v_{car} \end{bmatrix} \begin{bmatrix} \hat{\beta}_{bic} \\ \hat{r} \end{bmatrix} + \begin{bmatrix} b_1 - K_2 b_1 v_{car} \\ b_2 - K_4 b_1 v_{car} \end{bmatrix} \delta_f + \begin{bmatrix} K_1 & K_2 \\ K_3 & K_4 \end{bmatrix} \begin{bmatrix} r \\ a_y \end{bmatrix} \tag{7}$$

where $\hat{\beta}_{bic}$, $\hat{r}$, r and a_y are the estimated side slip angle, estimated yaw rate, sensor yaw rate measurement, and compensated lateral acceleration measurement, respectively.

Now, using the frozen-time pole-placement method, the observer gain K is selected to guarantee the observer system stability.

$$\begin{bmatrix} K_1 & K_2 \\ K_3 & K_4 \end{bmatrix} = \begin{bmatrix} \dfrac{I_z (C_f l_f - C_r l_r)}{2C_f C_r (l_f + l_r)^2} p_o^2 - 1 & \dfrac{1}{v_{car}} \\ -2p_o & \dfrac{m(C_f l_f^2 + C_r l_r^2)}{I_z (C_f l_f - C_r l_r)} \end{bmatrix}, \tag{8}$$

where p_o is a negative constant. For the sake of maintaining the system stability, the values of K_2 and K_4 are switched to zero as their denominators closely approach zero (Oh and Choi, 2011). The bicycle model observer thus estimates the vehicle lateral velocity using the following relationship.

$$\hat{v}_{y,bic} = v_{car} \tan \hat{\beta}_{bic} \tag{9}$$

where $\hat{v}_{y,bic}$ is the lateral velocity estimation obtained from the bicycle model-based observer.

4. DYNAMIC SENSOR ZEROING

4.1. Gyroscope Offset Compensation

The offset error compensation of the gyroscope sensors is relatively easy compared to that of the accelerometer, and this can be accounted by two characteristics of the vehicle angular rates. The first reason is that the gyroscope sensor signals are zero when the vehicle is at a stop, and the other reason is that the long term average of the vehicle angular rates are also zero. Exploiting these properties, the roll and pitch rate sensors can be easily adjusted as shown in the following for the sensor errors e_p and e_q.

$$p(t) = p^*(t) + e_p(t) \tag{10}$$

$$\dot{e}_p = \gamma_p[-e_p - p^*(t)] \tag{11}$$

$$q(t) = q^*(t) + e_q(t) \tag{12}$$

$$e_q = \gamma_q[-e_q - q^*(t)] \tag{13}$$

Here, $p^*(t)$ and $q^*(t)$ are the raw roll and pitch rate signals, whereas $p(t)$ and $q(t)$ are the processed ones. γ_p and γ_q are the positive tuning constants.

The second property may sound disputable in case of yaw rate, but the situation which involves a non-zero yaw rate can be easily discriminated in most of the cases by referring to the steering wheel angle, δ_f.

$$r(t) = r^*(t) + e_r \tag{14}$$

$$e_r = Z_r(t)\gamma_r[-e_r - r^*(t)] \tag{15}$$

where $Z_r(t) = \begin{cases} 1, |\delta_f| \le k_r \\ 0, |\delta_f| > k_r \end{cases}$

In the above compensation scheme, $r^*(t)$ is the measured raw yaw rate, whereas $r(t)$ is the processed one. γ_r and k_r are the positive tuning constants, and e_r is the estimated yaw rate sensor error.

A significant benefit of dynamically zeroing the gyroscope sensors is that, through applying the suggested algorithm with the time window, the compensation algorithm automatically adjusts the measurements even in cases of time-varying offset errors.

4.2. Accelerometer Offset Compensation

The accelerometer offset compensation is done over an extended period of time. Compared to how the gyroscope offset correction could be initiated simultaneously with starting the car, the accelerometer offset cannot be estimated the same way, since the gravitational force affects the accelerometer readings. In other words, the true accelerometer measurements are not necessarily zero (or 1 g in case of z-axis accelerometer) even when the vehicle is at a complete stop, if the vehicle is parked on a hill or a bank. For this reason, the accelerometer offset must be compensated dynamically as the vehicle engages in motion.

It is clear that the ideal sensor kinematics at the center of gravity in a vehicle follows the relationship shown next.

$$\begin{bmatrix} \dot{v}_x \\ \dot{v}_y \\ \dot{v}_z \end{bmatrix} = \begin{bmatrix} 0 & r & -q \\ -r & 0 & p \\ q & -p & 0 \end{bmatrix} \begin{bmatrix} v_x \\ v_y \\ v_z \end{bmatrix} + \begin{bmatrix} a_x + g \cdot \sin\theta \\ a_y - g \cdot \sin\phi \cdot \cos\theta \\ a_z - g \cdot \cos\phi \cdot \cos\theta \end{bmatrix} \tag{16}$$

In a practical sensor, however, when the offset errors for the acceleration measurements of each axis is considered, the state variables of the kinematics described in (16) would never converge to their true values. To resolve this issue, the basic idea of a disturbance observer is taken to perform the offset compensation for the accelerometer measurements, and the block diagram that describes the compensational scheme of the lateral dynamics is shown in Figure 1. Unlike other cases in which undesired disturbances exist within the real plant, the undesired offset error is mixed in the sensor inputs. Thus, the inverse kinematics is derived by solving (16) for acceleration, so that the offset can estimated.

$$a_x = \dot{v}_x - r \cdot v_y + q \cdot v_z - g \cdot \sin\theta \tag{17}$$

$$a_y = \dot{v}_y + r \cdot v_x - p \cdot v_z + g \cdot \sin\phi \cdot \cos\theta \tag{18}$$

$$a_z = \dot{v}_z - q \cdot v_x + p \cdot v_y + g \cdot \cos\phi \cdot \cos\theta \tag{19}$$

Here, it is assumed that $v_x = v_{car}$, $v_y = \hat{v}_{y,bic}$, $v_z = 0$, $\phi = 0$, and $\theta = 0$ since the long term average of the indicated vehicle states even out to zero. Such assumptions can be

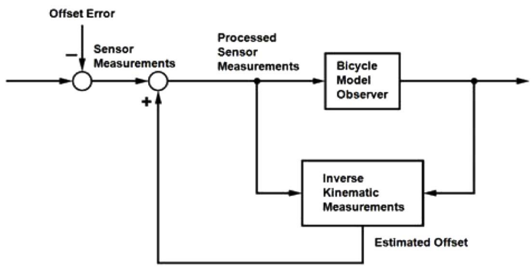

Figure 1. Block diagram representation of the accelerometer offset error compensation.

made based on the fact that, although sensors must be as accurate as possible at the moment of emergency to secure the vehicle safety through various safety control technologies, the time period of such moment is extremely brief relative to the time given for dynamic sensor zeroing.

Incorporating the above mentioned assumptions, the reference acceleration values can be defined as follows.

$$a_{x,ref} \equiv \dot{v}_w - r \cdot \hat{v}_{y,ref} \tag{20}$$

$$a_{y,ref} \equiv \dot{\hat{v}}_{y,ref} + r \cdot v_w \tag{21}$$

$$a_{z,ref} \equiv -q \cdot v_w + p \cdot \hat{v}_{y,ref} + g \tag{22}$$

By comparing the above values to the raw acceleration measurements, the raw signals $-a_x^*$, a_y^*, and a_z^* -are processed according to the following schemes.

$$a_x(t) = a_x^*(t) + e_x(t) \tag{23}$$

$$\dot{e}_x = Z_x(t)\gamma_x[-e_x + (a_{x,ref} - a_x^*)] \tag{24}$$

where $Z_x(t) = \begin{cases} 1, \text{x-axis dynamic sensor zeroing condition} \\ 0, \text{otherwise} \end{cases}$

$$a_y(t) = a_y^*(t) + e_y(t) \tag{25}$$

$$\dot{e}_y = Z_y(t)\gamma_y[-e_y + c_y(a_{y,ref} - a_y^*)] \tag{26}$$

where $Z_z(t) = \begin{cases} 1, \text{y-axis dynamic sensor zeroing condition} \\ 0, \text{otherwise} \end{cases}$

$$a_z(t) = a_z^*(t) + e_z(t) \tag{27}$$

$$\dot{e}_z = Z_z(t)\gamma_z[-e_z + (a_{z,ref} - a_z^*)] \tag{28}$$

where $Z_z(t) = \begin{cases} 1, \text{z-axis dynamic sensor zeroing condition} \\ 0, \text{otherwise} \end{cases}$

Here, γ_x, γ_y, c_y, and γ_z are the positive tuning constants, with $c_y > 1$. The indices to switch between the dynamic sensor zeroing mode and hold mode exist for the offset compensation of the sensors arranged for each axis. The reasoning behind incorporating such indices is to ensure that the reference acceleration values are reliable. In other words, the dynamic sensor zeroing condition should only include the situation in which the assumptions claimed for the calculation of the reference acceleration values hold.

Now a variance-like variable, τ, which represents the degree of transient motion of the vehicle, is defined as shown next.

$$\tau \equiv \sum_{i=1}^{7} \left\{ \frac{k_i \int_t^{t+\Delta t_i} \left(x_i - \frac{\int_t^{t+\Delta t_i} x_i d\tau}{\Delta t_i} \right)^2 d\tau}{\Delta t_i} \right\} \tag{29}$$

Table 3. Dynamic sensor zeroing conditions.

	τ	v_{car}	δ_f	r
x-axis DSZ condition	$\tau < c_1$	$\mathrm{Var}(v_{car}) < c_2$		
y-axis DSZ condition		$v_{car} > c_3$	$\lvert\delta_f\rvert < c_4$ $\mathrm{Var}(\delta_f) < c_5$	$\lvert r\rvert < c_6$
z-axis DSZ condition	$\tau < c_7$			

$c_1 \sim c_7$: tuning parameters

Using (29), the dynamic sensor zeroing condition is defined, and these conditions are sorted in Table 3.

5. STABILITY ANALYSIS

This section deals with the stability verification of the accelerometer offset compensation algorithm. Since the gyroscope offset compensation process subtracts the mean signal deviation with respect to zero, divergence of the system is unlikely to happen. However, in case of the accelerometer, especially for the lateral acceleration, stability of the system must be guaranteed, because the offset compensation is performed with respect to the reference signal generated by the inverse kinematics, which utilizes the lateral velocity. In other words, failure to maintain system stability may induce the bicycle model based observer estimation of the lateral velocity and the lateral acceleration measurement with offset to mutually influence each other to cause divergence. On the other hand, importance of the stability verification related to the longitudinal and vertical accelerations is trivial, since they utilize open loop information of v_{car}, and bicycle model observer is decoupled from the a_z compensation scheme.

Recall (8) for the stability verification. The error dynamics of the lateral acceleration offset value must be considered along with the bicycle model observer dynamics which estimates the lateral velocity. Here, stability analysis is done for the condition in which $Z_y(t) = 1$, i.e. when the dynamic sensor zeroing process of the lateral acceleration is switched on, because that is when the lateral vehicle dynamics and the compensational schemes are coupled together.

$$\begin{bmatrix} \dot{\hat{\beta}}_{bic} \\ \dot{\hat{r}} \\ \dot{e}_y \end{bmatrix} = \begin{bmatrix} a_{11} - K_2 a_{11} v_{car} & a_{12} - K_1 - K_2(a_{12}+1)v_{car} & K_2 \\ a_{21} - K_4 a_{11} v_{car} & a_{22} - K_3 - K_4(a_{12}+1)v_{car} & K_4 \\ 0 & 0 & -\gamma_y \end{bmatrix} \begin{bmatrix} \hat{\beta}_{bic} \\ \hat{r} \\ e_y \end{bmatrix} + \begin{bmatrix} b_1 - K_2 b_1 v_{car} \\ b_2 - K_4 b_1 v_{car} \\ 0 \end{bmatrix} \delta_f + \begin{bmatrix} K_1 & K_2 & 0 \\ K_3 & K_4 & 0 \\ c_y\gamma_y \cdot v_{car} & -c_y\gamma_y & 1 \end{bmatrix} \begin{bmatrix} r \\ a_y^* \\ c_y\gamma_y v_{car}\dot{\hat{\beta}}_{bic} \end{bmatrix} \tag{30}$$

Here, (30) shows the observer system which has merged the bicycle model observer and the lateral accelerometer error dynamics. Rearranging the above relationship gives the following.

$$\begin{bmatrix}\dot{\hat{\beta}}_{bic}\\ \dot{\hat{r}}\\ \dot{\hat{e}}_y\end{bmatrix} = \left\{\begin{bmatrix} a_{11}-K_2a_{11}v_{car} & \begin{matrix}a_{12}-K_1\\ -K_2\left(a_{12}+1\right)v_{car}\end{matrix} & K_2 \\ a_{21}-K_4a_{11}v_{car} & \begin{matrix}a_{22}-K_3\\ -K_4\left(a_{12}+1\right)v_{car}\end{matrix} & K_4\\ \begin{matrix}c_y\gamma_y v_{car}\cdot\\ \begin{pmatrix}a_{11}\\ -K_2a_{11}v_{car}\end{pmatrix}\end{matrix} & \begin{matrix}c_y\gamma_y v_{car}\cdot\\ \begin{pmatrix}a_{12}-K_1\\ -K_2\left(a_{12}+1\right)v_{car}\end{pmatrix}\end{matrix} & \begin{matrix}c_y\gamma_y v_{car}K_2\\ -\gamma_y\end{matrix}\end{bmatrix}\cdot\begin{bmatrix}\hat{\beta}_{bic}\\ \hat{r}\\ \hat{e}_y\end{bmatrix}\right\} + \begin{bmatrix} b_1-K_2b_1v_{car}\\ b_2-K_4b_1v_{car}\\ c_y\gamma_y v_{car}b_1 - c_y\gamma_y v_{car}K_2b_1v_{car}\end{bmatrix}\delta_f + \begin{bmatrix}K_1 & K_2\\ K_3 & K_4\\ c_y\gamma_yv_{car}K_1 + c_y\gamma_y\cdot v_{car} & c_y\gamma_yv_{car}K_2 - c_y\gamma_y\end{bmatrix}\begin{bmatrix} r\\ a_y^{*}\end{bmatrix} \tag{31}$$

This can be compared to the ideal system shown next.

$$\begin{bmatrix}\dot{\beta}_{bic}\\ \dot{r}\\ \dot{e}_y\end{bmatrix} = \begin{bmatrix}a_{11}&a_{12}&0\\a_{21}&a_{22}&0\\0&0&0\end{bmatrix}\begin{bmatrix}\beta_{bic}\\ r\\ e_y\end{bmatrix}+\begin{bmatrix}b_1\\b_2\\0\end{bmatrix}\delta_f \tag{32}$$

There is no dynamics involved in e_y, since it is assumed that the ideal e_y is slowly varying. Now to compare the observer estimation with the real states, the errors are defined.

$$\begin{bmatrix}\dot{\tilde{\beta}}_{bic}\\ \dot{\tilde{r}}\\ \dot{\tilde{e}}_y\end{bmatrix} \square \begin{bmatrix}\beta_{bic}-\dot{\hat{\beta}}_{bic}\\ \dot{r}-\dot{\hat{r}}\\ \dot{e}_y-\dot{e}_y\end{bmatrix} \tag{33}$$

With the above, the following error dynamics is reached.

$$\begin{bmatrix}\dot{\tilde{\beta}}_{bic}\\ \dot{\tilde{r}}\\ \dot{\tilde{e}}_y\end{bmatrix} = \begin{bmatrix}K_2a_{11}v_{car} & K_1+K_2\left(a_{12}+1\right)v_{car} & -K_2\\ K_4a_{11}v_{car} & K_3+K_4\left(a_{12}+1\right)v_{car} & -K_4\\ 0 & -c_y\gamma_yv_{car}\begin{pmatrix}a_{12}-K_1\\ -\left(a_{12}+1\right)\end{pmatrix} & \gamma_y\left(1-c_y\right)\end{bmatrix}\begin{bmatrix}\tilde{\beta}_{bic}\\ \tilde{r}\\ \tilde{e}_y\end{bmatrix} + \begin{bmatrix}0\\ K_4b_1v_{car}\\ 0\end{bmatrix}\delta_f + \begin{bmatrix}-K_1 & -K_2\\ -K_3 & -K_4\\ -c_y\gamma_yv_{car}K_1 - c_y\gamma_y\cdot v_{car} & 0\end{bmatrix}\begin{bmatrix}r\\ a_y^{*}\end{bmatrix} \tag{34}$$

Through an investigation on the state matrix, it turns out that it is Hurwitz. Hence, it shows the stability of the combined zero-input system. Mere zero-input stability, however, does not guarantee the ideal offset compensation of the sensor measurements. So (34) is further extended to have the steady state analysis obtained.

At a steady state, it is assumed that there is no change in the states, so the following relationship holds.

$$\begin{bmatrix}0\\0\\0\end{bmatrix} = \begin{bmatrix}K_2a_{11}v_{car} & K_1+K_2\left(a_{12}+1\right)v_{car} & -K_2\\ K_4a_{11}v_{car} & K_3+K_4\left(a_{12}+1\right)v_{car} & -K_4\\ 0 & -c_y\gamma_yv_{car}\begin{pmatrix}a_{12}-K_1\\ -\left(a_{12}+1\right)\end{pmatrix} & \gamma_y\left(1-c_y\right)\end{bmatrix}\begin{bmatrix}\tilde{\beta}_{bic}\\ \tilde{r}\\ \tilde{e}_y\end{bmatrix} + \begin{bmatrix}-K_1 & -K_2\\ -K_3 & -K_4\\ -c_y\gamma_yv_{car}K_1 - c_y\gamma_y\cdot v_{car} & 0\end{bmatrix}\begin{bmatrix}r\\ a_y^{*}\end{bmatrix} \tag{35}$$

In order to solve for the state errors, the above relationship is put into an augmented matrix and row operations are applied to reach the echelon form.

$$\left[\begin{array}{ccc|c}K_2a_{11}v_{car} & K_1+K_2\begin{pmatrix}a_{12}\\+1\end{pmatrix}v_{car} & -K_2 & K_1r+K_2a_y^{*}\\ K_4a_{11}v_{car} & K_3+K_4\begin{pmatrix}a_{12}\\+1\end{pmatrix}v_{car} & -K_4 & K_3r+K_4a_y^{*}\\ 0 & -c_y\gamma_yv_{car}\begin{pmatrix}a_{12}-K_1\\ -\left(a_{12}+1\right)\end{pmatrix} & \gamma_y\left(1-c_y\right) & c_y\gamma_yv_{car}\left(-K_1-1\right)r\end{array}\right]$$
$$\sim\left[\begin{array}{ccc|c}K_2a_{11}v_{car} & K_1+K_2\begin{pmatrix}a_{12}\\+1\end{pmatrix}v_{car} & -K_2 & K_1r+K_2a_y^{*}\\ 0 & K_3-\frac{K_4}{K_2}K_1 & 0 & \left(K_3-\frac{K_4}{K_2}K_1\right)r\\ 0 & \begin{matrix}-c_y\gamma_yv_{car}\cdot\\ \begin{pmatrix}a_{12}-K_1\\ -\left(a_{12}+1\right)\end{pmatrix}\end{matrix} & \gamma_y\left(1-c_y\right) & c_y\gamma_yv_{car}\left(-K_1-1\right)r\end{array}\right] \tag{36}$$
$$\sim\left[\begin{array}{ccc|c}K_2a_{11}v_{car} & K_1+K_2\begin{pmatrix}a_{12}\\+1\end{pmatrix}v_{car} & -K_2 & K_1r+K_2a_y^{*}\\ 0 & K_3-\frac{K_4}{K_2}K_1 & 0 & \left(K_3-\frac{K_4}{K_2}K_1\right)r\\ 0 & 0 & \gamma_y\left(1-c_y\right) & 2c_y\gamma_yv_{car}\left(-K_1-1\right)r\end{array}\right]$$

From the result obtained in (36), it is straight forward to obtain the steady state errors of the states.

$$\tilde{e}_y\big|_{ss} = \frac{2c_y\gamma_yv_{car}(-K_1-1)r}{\gamma_y(1-c_y)} \tag{37}$$

$$\tilde{r}\big|_{ss} = r \tag{38}$$

$$\tilde{\beta}_{bic}\big|_{ss} = \frac{K_1r+K_2a_y^{*}+K_2\tilde{e}_{y,ss}-(K_1+K_2(a_{12}+1)v_{car})\tilde{r}}{a_{11}} \tag{39}$$

Now recall Table 3, which states that the condition $Z_y(t) = 1$ is met when the corrected yaw rate is close to zero. This indicates that the steady state errors approach zero as long as the sensor offset compensation is at work.

6. EXPERIMENT RESULTS

6.1. Test Environments

Given in Table 4 is the specification data of the SUV, Hyundai Tucsan ix, that was used for the experiment to show the 6D IMU offset error compensation performance.

Also, Table 5 shows the relative distance between the instruments mounted on the test vehicle. Here, a GPS/INS system of RT3000 class (specific model: RT3100) from the Oxford Technical Solutions Ltd. is used for the verification purpose, and the measurements taken by RT3000 is assumed to be the actual values.

6.2. Test with Sine Steer Maneuver

Figure 2 shows the 6D IMU measurements taken during the sine steer maneuver on the flat dry surface of asphalt. Between the measurements taken by the RT3000 sensor and that taken by the raw 6D IMU, significant amount of offset errors can be clearly observed. Along with these signals, the processed 6D IMU signals are compared, and it is evident that these signals are closer to the RT3000 measurements.

Table 4. Test vehicle specification.

Tucsan ix 2WD gasoline theta II 2.0 specification					
Feature		Front		Rear	
		Left	Right	Left	Right
Dimension [mm]	Wheelbase	2640			
	Overhang	800		890	
	Track	1585		1586	
	Overall length	4410			
	Overall width	1820			
	Height (unloaded)	1655			
Weight [kgf]	Curb weight	450	417	326	330
		867		656	
		1523			
	Gross vehicle weight (2 up)	487	458	360	368
		945		728	
		1673			
Wheel radius [mm]		336	338	340	340
		337		340	

Table 5. Instruments mounting positions.

Distance between instruments		Distance [mm]
Length (X-axis)	RT3100~rear axle center	1000
	RT3100~6D IMU	930
Height (Z-axis)	RT3100~antenna	600
	RT3100~6D IMU	430

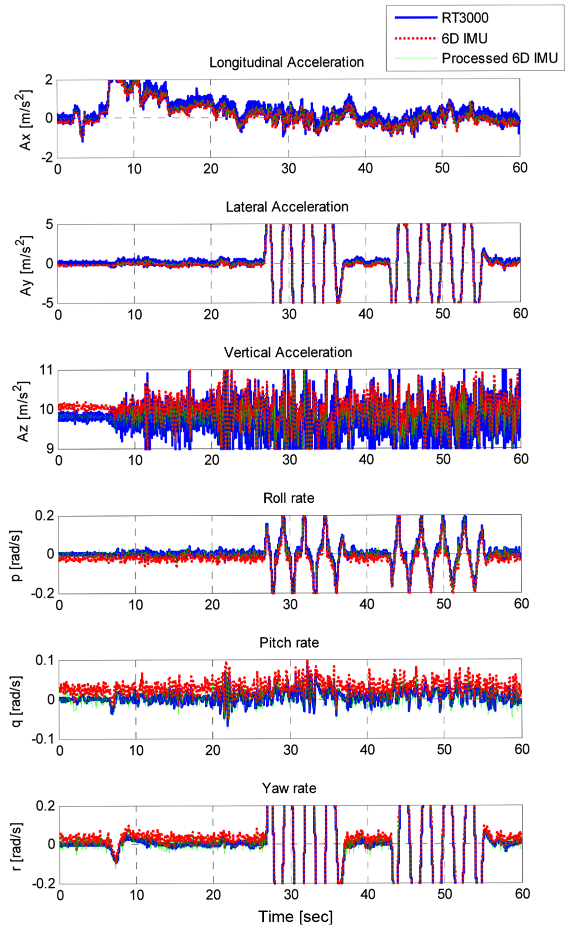

Figure 2. 6D IMU measurements during sine steer test.

Figure 3 displays a magnified portion of what is shown in Figure 2 during the time period 10~14 seconds.

Here, in Figure 3, it must be noted that the processed lateral acceleration measurement is not much different from the raw signal in the earlier part, but the effect of compensation eventually causes the processed signal to be much closer to the real value. This is accounted by the changing $Z_y(t)$ from stop mode to the dynamic sensor zeroing mode. Thus, although it may be impossible to correctly zero the acceleration values at the moment the car starts, it is possible to compensate the offset error as the vehicle engages in motion.

The reference acceleration values obtained from the inverse kinematics is displayed in Figure 4. As expected, a general decrease in accuracy and reliability of the reference values is detected whenever the vehicle engages in a series of sine steer maneuvers.

By discarding the reference acceleration information obtained in this phase, and only exploiting it when the aforementioned conditions are satisfied, robust compensa-

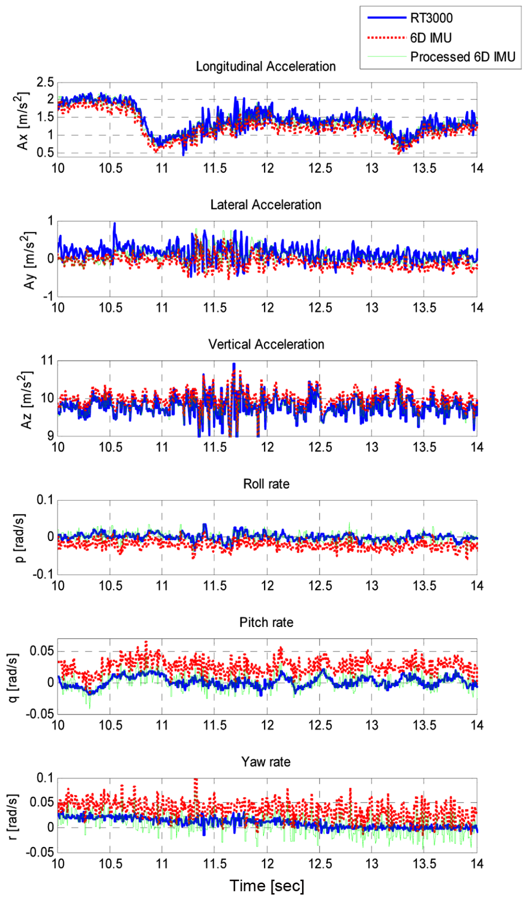

Figure 3. Magnified 6D IMU measurements during sine steer test.

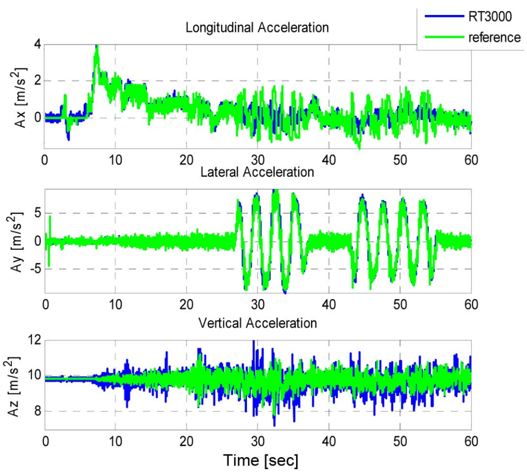

Figure 4. Reference accelerations for sine steer test.

tion performance can be reached. A clearer discrepancy between the reliability of the reference signals is shown in the test results exhibited in the following section.

The plot in Figure 5 displays the RMS errors of both raw and processed 6D IMU measurements relative to the

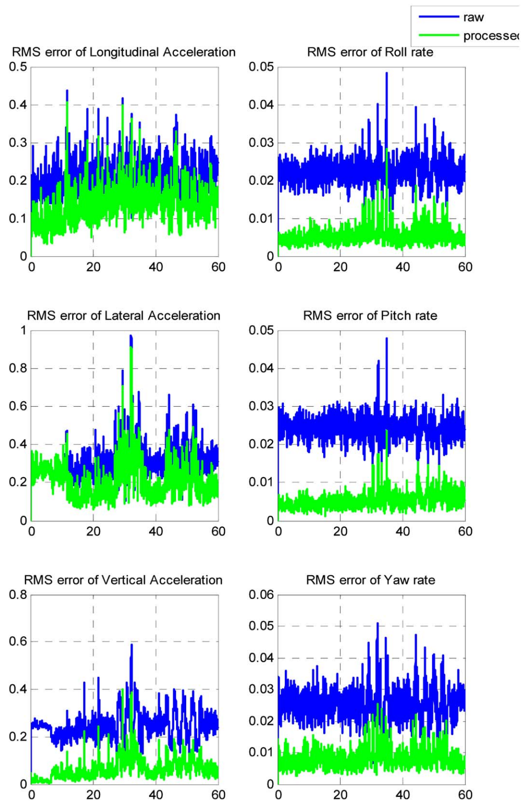

Figure 5. RMS errors of the 6D IMU measurements.

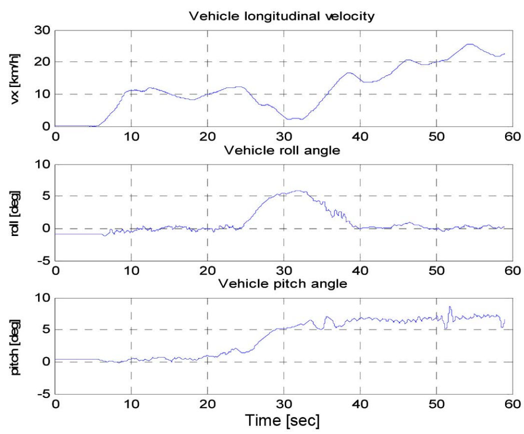

Figure 6. Test conditions.

measurements taken by RT3000 sensor. It apparently indicates that the RMS errors of the processed signals are lower than that of the raw signals. It must be clarified that the error values of the processed signals do not come from the remaining offset error, but rather come majorly from the noise component, whose influence on the vehicle state estimation is significantly less than that of the offset errors.

6.3. Test with Static Bank and Inclination Angles

In the second part of the experiment, the vehicle is tested

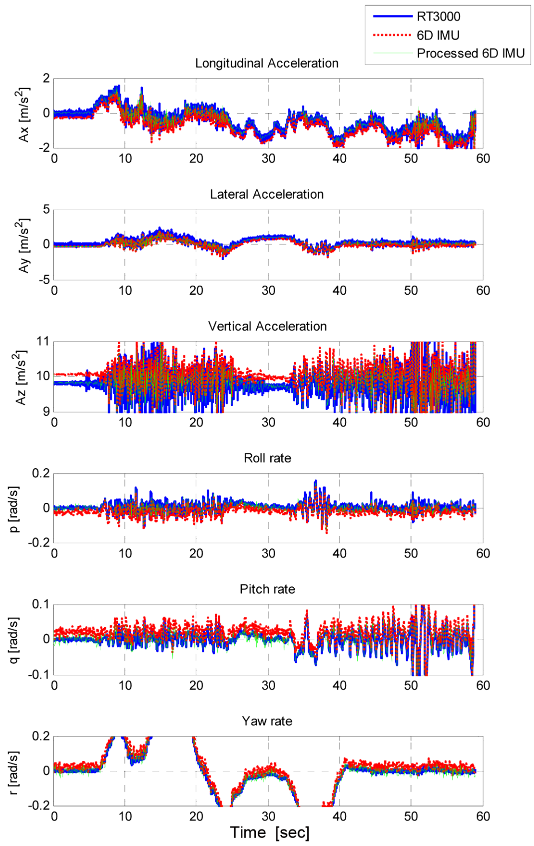

Figure 7. 6D IMU measurements on uneven terrain.

under the road conditions with a fairly severe longitudinal and lateral inclination angles.

Figure 6 shows the longitudinal vehicle velocity, vehicle roll, and pitch angles. They indicate that the vehicle moves on a constant downhill of more than 6 degrees starting from about 25 second, and a static bank angle of nearly 6 degrees exist on its way as well.

Figure 7 shows the raw and processed 6D IMU measurements in comparison with the RT3000 sensor measurements. Again, it can be seen that a significant amount of offset error is eliminated from the raw measurements.

Figure 8 shows the magnified portion of what is shown in Figure 7, and analogous to the previous test scenario, the beginning stage of the dynamic sensor zeroing can clearly be seen in the lateral acceleration measurements around 20.9 seconds.

Now Figure 9 is the magnified portion of Figure 7 that focuses on the part where the vehicle is on the road with both longitudinal and lateral static angles. Knowing that dynamic sensor zeroing is the most tedious under the condition with uneven road terrain, it is relieving to verify that the compensational work is unaffected by the road terrain.

The next plot in Figure 10 shows the clear decrease in

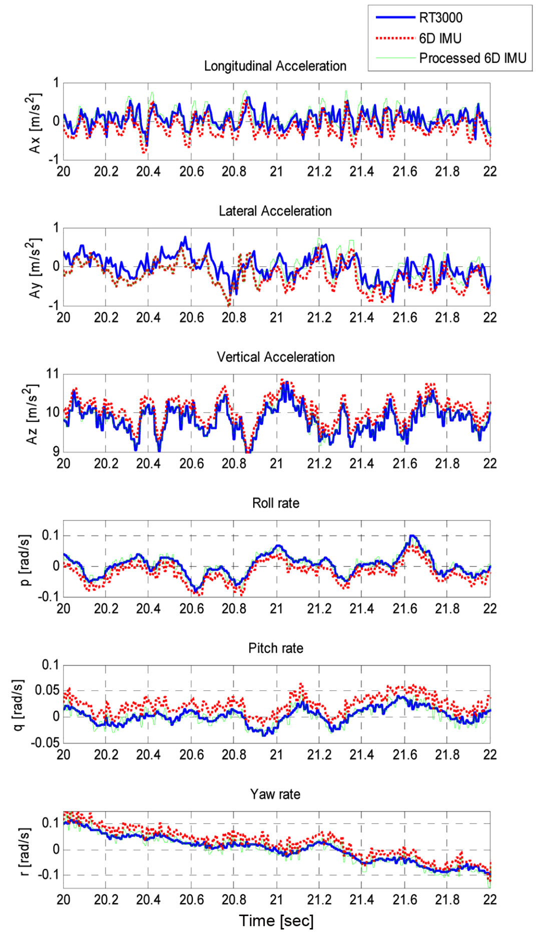

Figure 8. Magnified 6D IMU measurements on uneven terrain.

the reliability of the reference signals in the existence of the severe roll and pitch angles, but they are well filtered out to maintain what has been compensated previously.

Finally, Figure 11 shows the RMS errors of the raw and processed 6D IMU measurements for the test scenario with even road terrain. It again clearly indicates that the error range of the IMU measurements has been significantly brought down through the dynamic sensor zeroing algorithm.

7. CONCLUSION

A novel vehicle 6D IMU sensor signal compensation scheme for the steady state offset error is suggested. Independence from using GPS signal appeals the uniqueness of the designed algorithm. By using the bicycle model-based observer, the range of dynamic sensor zeroing is expanded, so that the time required for the robust sensor zeroing is reduced significantly. Here, the stability of the coupled lateral dynamic system is deliberately proved, so that the sensor offset error is accurately estimated.

The above methodology is tested with a real production

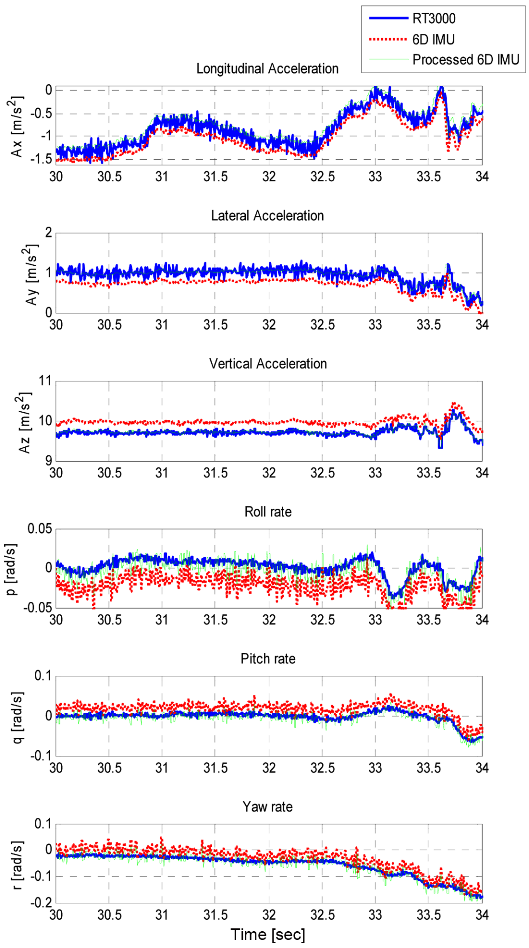

Figure 9. Magnified 6D IMU measurements on static bank and inclination.

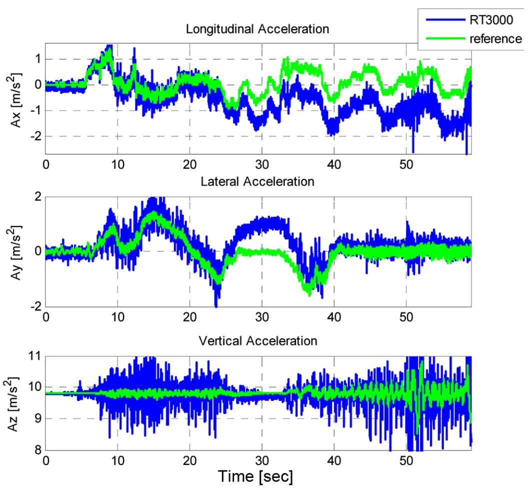

Figure 10. Reference accelerations on uneven terrain.

SUV to prove its worthiness. The experiments are conducted under various conditions, and the test results show that, regardless of the severity of steering input and the existence

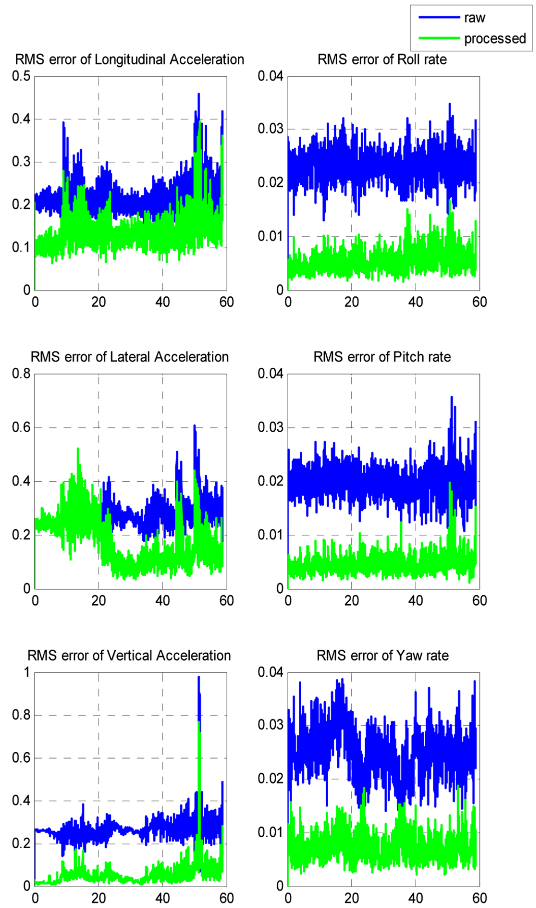

Figure 11. RMS errors of the 6D IMU measurements.

of road angles, the sensor compensation algorithm is reasonably robust and accurate.

ACKNOWLEDGEMENT–The authors would like to thank S. H. You, J. Y. Seo, and S. G. Kang of Hyundai Motor co. for their tireless efforts in developing the contents. This document has its origin in the X-by-wire Project, without which this study could not have been completed.

REFERENCES

Abdel-Hamid, W., Abdelazim, T., El-Sheimy, N. and Lachapelle, G. (2006). Improvement of MEMS-IMU/GPS performance using fuzzy modeling. *GPS Solution* **10**, **2**, 1–11.

Begin, J. D. and Cheok, K. C. (1998). Calibration of Multi-axis Accelerometer in Vehicle Navigation System. U.S. Patent 6532419.

Cho, S. Y. and Choi, W. S. (2005). A robust positioning technique in DR/GPS using the receding horizon sigma point Kalman FIR filter. *Proc. IEEE IMTC 2005*, 1354–1359.

Cho, S. Y. and Choi, W. S. (2006). Performance enhancement of low-cost land navigation for location based service. *ETRI J.* **28**, **2**, 131−144.

Kim, S. B., Choi, K. H., Lee, S. Y., Choi, J. H., Hwang, T. H., Jang, B. T. and Lee, J. H. (2004). A bimodal approach for land vehicle localization. *ETRI J.* **26**, **5**, 497−500.

Li, Y., Wang, J., Rizos, C., Baitch, G. and Kinlyside, D. (2005). Application of GPS/INS integration technique to bushfire monitoring. *Spatial Sciences Conf.*, Melbourne, Australia, 1394−1403.

Noureldin, A., Karamat, B., Eberts, M. D. and El-Shafie, A. (2009). Performance enhancement of MEMS-based INS/GPS integration for low-cost navigation applications. *IEEE Trans. Vehicular Technology* **58**, **3**, 1077−1096.

Oh, J. and Choi, S. B. (2011). Design of a new composite observer for vehicle velocity and attitude estimation. *Proc. IASTED Int. Conf., Control and Applications*, Vancouver, BC, Canada, 102−109.

Oh, J., Noh, Y. and Choi, S. B. (2013). Real-time offset error compensation of 6D IMU mounted on ground vehicles using disturbance observer. *Int. Conf. Intelligent Information and Networks*, Male, Maldives.

Rogers, R. M. (1997). IMU in-motion alignment without benefit of attitude initialization, navigation. *J. Institute of Navigation* **44**, **3**, 301−311.

Shin, E. H. (2001). Accuracy Improvement of Low Cost INS/GPS for Land Applications. *UCGE Reports* Number 20156, The University of Calgary, Calgary, Alberta, Canada.

Shin, E. H. and El-Sheimy, N. (2004). An unscented Kalman filter for in-motion alignment of low-cost IMUs. *Proc. IEEE Frames Conf.*, 273−279.

Son, H. W. (2008). A study on design of a robust vehicle side-slip angle observer using an integration of kinematic and bicycle model. *KSAE 2008 Annual Conf.*, Daejeon, Korea.

Tanaka, H. and Kazumi, Y. (1996). Gravitational Accelerometer Provided with Zero Adjuster. U.S. Patent 5526263.

You, S. H., Hahn, J. O. and Lee, H. C. (2009). New adaptive approaches to real-time estimation of vehicle sideslip angle. *Control Engineering Practice* **17**, **12**, 1367−1379.

APPENDIX

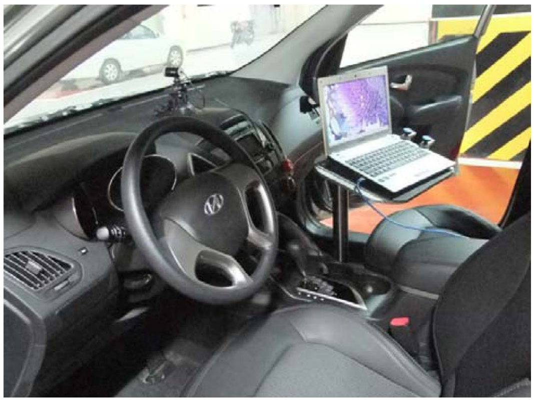

Apparatus for experiments (Interior)

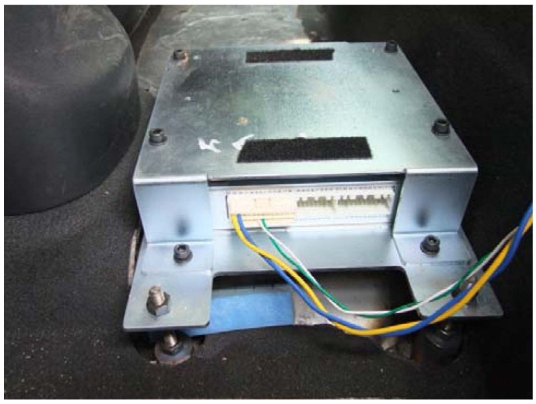

6D IMU

RT3100